

HEALTH AND MEDICINE

Poly(vinyl alcohol) boosting therapeutic potential of *p*-boronophenylalanine in neutron capture therapy by modulating metabolism

Takahiro Nomoto^{1*†}, Yukiya Inoue^{1†}, Ying Yao¹, Minoru Suzuki², Kaito Kanamori¹, Hiroyasu Takemoto¹, Makoto Matsui¹, Keishiro Tomoda¹, Nobuhiro Nishiyama^{1,3*}

In the current clinical boron neutron capture therapy (BNCT), *p*-boronophenylalanine (BPA) has been the most powerful drug owing to its ability to accumulate selectively within cancers through cancer-related amino acid transporters including LAT1. However, the therapeutic success of BPA has been sometimes compromised by its unfavorable efflux from cytosol due to their antiport mechanism. Here, we report that poly(vinyl alcohol) (PVA) can form complexes with BPA through reversible boronate esters in aqueous solution, and the complex termed PVA-BPA can be internalized into cancer cells through LAT1-mediated endocytosis, thereby enhancing cellular uptake and slowing the untoward efflux. In *in vivo* study, compared with clinically used fructose-BPA complexes, PVA-BPA exhibited efficient tumor accumulation and prolonged tumor retention with quick clearance from bloodstream and normal organs. Ultimately, PVA-BPA showed critically enhanced antitumor activity in BNCT. The facile technique proposed in this study offers an approach for drug delivery focusing on drug metabolism.

INTRODUCTION

Boron neutron capture therapy (BNCT) uses nuclear fission reaction between a boron atom (¹⁰B) and a low-energy thermal neutron, generating a high linear energy transfer (LET) α particle and a Li recoil nucleus that induce strong cytotoxic effect to cancer cells (1–3). Since the ranges of the α particle and Li nucleus are within 10 μ m, successful BNCT requires selective delivery of ¹⁰B to targeted cancer cells. In 1987, Mishima *et al.* demonstrated the first clinical success of BNCT on a malignant melanoma using *p*-boronophenylalanine (BPA) (Fig. 1A), and BPA has since been the most useful drug in clinical neutron capture therapy (4). BPA has the structure of phenylalanine that can be recognized mainly by LAT1 amino acid transporters overexpressed on many cancer cells, thereby permitting efficient cellular internalization (5, 6). In addition, fluorinated BPA (¹⁸F-BPA) was recently developed for companion diagnostics, and it has been experimentally demonstrated that ¹⁸F-BPA exhibits similar biodistribution to the unfluorinated BPA (7, 8) and allows us to quantitatively illustrate tumor accumulation of BPA and select patients who are likely to receive benefit from BNCT (9).

Although BPA has the above advantages, its clinical usage has been hampered by poor water solubility (10) and short retention time in tumors (11). The former poor water solubility is thought to originate from the chemical structure of BPA, as it has hydrophobic structure of phenylalanine and neutral charge at physiological pH, making intermolecular salts that are difficult to dissolve (10). While BPA-hydrochloride solution at low pH was used in the beginning

of its clinical application, Yoshino and co-workers (10) found that sugars including fructose can form complexes with boronic acids in BPA and increase the water solubility. Thus, recent clinical studies have used fructose as a solubilizer. However, the problem of short retention time in tumors remains to be solved. As previously mentioned, BPA can quickly and efficiently accumulate within a target tumor, but BPA concentration gradually decreases during irradiation of thermal neutrons that usually requires 30 to 60 min, compromising the therapeutic potential of BPA. Currently, fructose-BPA is infused to patients even during irradiation of epi-/thermal neutrons to maintain high intratumoral boron concentration (12). This technique has successfully improved the therapeutic potential of BPA; however, it brings with it the possibility of human errors, such as dislodgement of the injection needle in the middle of the irradiation. In addition, the complicated settings required for infusion limits the number of treatments per neutron source. Hence, suppressing efflux of intratumoral BPA should be key to optimizing the clinical outcome of BNCT.

One possible explanation for the short retention is the antiport mechanism of amino acid transporters including LAT1. When LAT1 imports an extracellular substrate (for example, BPA) into the cytosol, it also exports an intracellular substrate such as glutamine (Fig. 1B). In a similar way, if the extracellular BPA concentration is decreased, intracellular BPA should be exchanged with an extracellular amino acid (Fig. 1C) (5). In line with this possible mechanism, a previous study reported that preadministration of substrates of LAT1 enhanced tumor accumulation of BPA (13), and another study demonstrated that preloading of BPA in cancer cells augmented the cellular uptake of ¹⁸F-BPA (14), indicating that both extracellular and intracellular BPA molecules should be subject to the antiport mechanism of LAT1. Considering these backgrounds, we hypothesized that modulation of subcellular localization of BPA should prevent intracellular BPA from untoward export by the antiport mechanism.

Here, to examine our hypothesis, we mixed poly(vinyl alcohol) (PVA) and BPA in aqueous solution, forming complexes via reversible boronate esters as illustrated in Fig. 1D. The complex formation does not affect the structure of phenylalanine in BPA; thus, the complex

¹Laboratory for Chemistry and Life Science, Institute of Innovative Research, Tokyo Institute of Technology, 4259 Nagatsutacho, Midori-ku, Yokohama, Kanagawa 226-8503, Japan. ²Division of Particle Radiation Oncology, Particle Radiation Oncology Research Center, Institute for Integrated Radiation and Nuclear Science, Kyoto University, 2-1010 Asashiro-nishi, Kumatori-cho, Sennan-gun, Osaka 590-0494, Japan. ³Innovation Center of Nanomedicine, Kawasaki Institute of Industrial Promotion, 3-25-14 Tonomachi, Kawasaki-ku, Kawasaki, Kanagawa 210-0821, Japan.

*Corresponding author. Email: nomoto@res.titech.ac.jp (T.N.); nishiyama.n.ad@m.titech.ac.jp (N.N.)

†These authors contributed equally to this work.

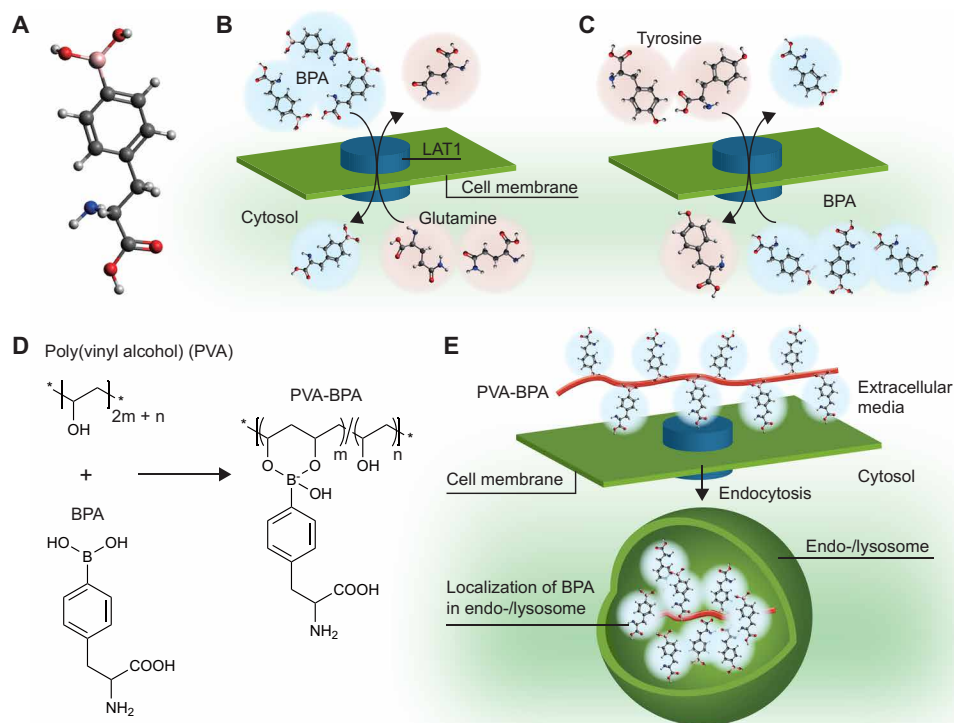


Fig. 1. Schematic illustration of influx and efflux of BPA. (A) Molecular structure of BPA (white-, gray-, red-, blue-, and pink-colored atoms are H, C, O, N, and B, respectively). (B) Cell internalization of BPA through the LAT1 transporter. LAT1 imports extracellular BPA and exports intracellular substrates including glutamine. (C) Efflux of intracellular BPA. When extracellular concentration of BPA decreases, intracellular BPA could be exchanged with an extracellular substrate including tyrosine. (D) Chemical structure of PVA and PVA-BPA. PVA-BPA formation does not involve phenylalanine structure in BPA, which is critical for recognition by LAT1. (E) Internalization pathway of PVA-BPA. PVA-BPA is expected to interact with LAT1, followed by internalization through endocytosis.

is expected to be recognized by LAT1 similarly to BPA alone. However, the PVA-BPA complex is unlikely to pass the LAT1 transporter due to its macromolecular structure and is likely to be internalized into the cell through LAT1-mediated endocytosis, thereby resulting in localization in endo-/lysosomes (Fig. 1E). The BPA trapped in endo-/lysosomes may not be subject to the antiport mechanism of LAT1 on the cell membrane, thereby slowing untoward efflux from the intracellular region. Our results indicate that the alteration of the internalization pathway and subcellular localization could enhance intracellular retention of BPA in cultured cells. Even in a subcutaneous tumor model, compared with clinically used fructose-BPA complexes, PVA-BPA exhibited augmented accumulation and prolonged retention within a tumor and exerted significantly enhanced antitumor effects upon neutron irradiation. Simple use of PVA as a solubilizer can therefore drastically enhance the therapeutic potential of BPA.

RESULTS

Construction of PVA-BPA

PVA ($M_n = 9500$) was synthesized by saponification of poly(vinyl acetate) (PVAc) ($M_w/M_n = 1.31$) that was synthesized using reversible addition-fragmentation chain transfer (RAFT) polymerization as shown in fig. S1. The saponification rate was estimated to be approximately 99% by ^1H nuclear magnetic resonance (NMR) spectroscopy. The characterizations of PVAc and PVA by gel permeation chromatography (GPC) and ^1H NMR spectroscopy are shown in figs. S2 to S5. PVA-BPA was then constructed by simple mixing of

PVA and BPA in aqueous solution. The formation of the complex was confirmed by ^{11}B NMR analysis (fig. S6), in which the complex formation induced a shift and broadening of signal from ^{11}B in BPA.

Cellular internalization pathway

To examine whether PVA-BPA is internalized into cells through endocytosis, we observed subcellular localization of PVA-BPA in cultured BxPC-3 cells expressing LAT1 transporter using confocal laser scanning microscopy (CLSM) (Fig. 2A). The cells were incubated with clinically used fructose-BPA or Cy5-labeled PVA-BPA (Cy5-PVA-BPA) for 30 min, and BPA was visualized using a fluorescent boronic acid sensor [5-(diethylamino)-2-((methylimino)methyl)phenol (DAHMI)] developed by Hattori *et al.* (15, 16). Consistent with a previous study (16), fructose-BPA was detected in the whole cell, indicating its localization in the cytosol through LAT1. By contrast, PVA-BPA was localized in endo-/lysosomes, which is highlighted by the white signals: the overlap of red (Cy5-PVA), green (LysoTracker Red DND-99), and blue (BPA-DAHMI) signals. These results suggest that PVA-BPA was internalized into cells via endocytosis. Note that PVA-BPA-treated cells also showed localization of some BPA in the cytosol without Cy5 fluorescence. The presence of BPA in the cytosol suggests that some of the BPA molecules dissociated from PVA-BPA complexes could be internalized through LAT1 transporters. In addition, sole Cy5 fluorescence could be observed on the cell surface in the CLSM image of PVA-BPA. Because DAHMI emits strong fluorescence upon reaction with boronic acid, complex formation of BPA with PVA might inhibit the detection of BPA with DAHMI. However, an acidic

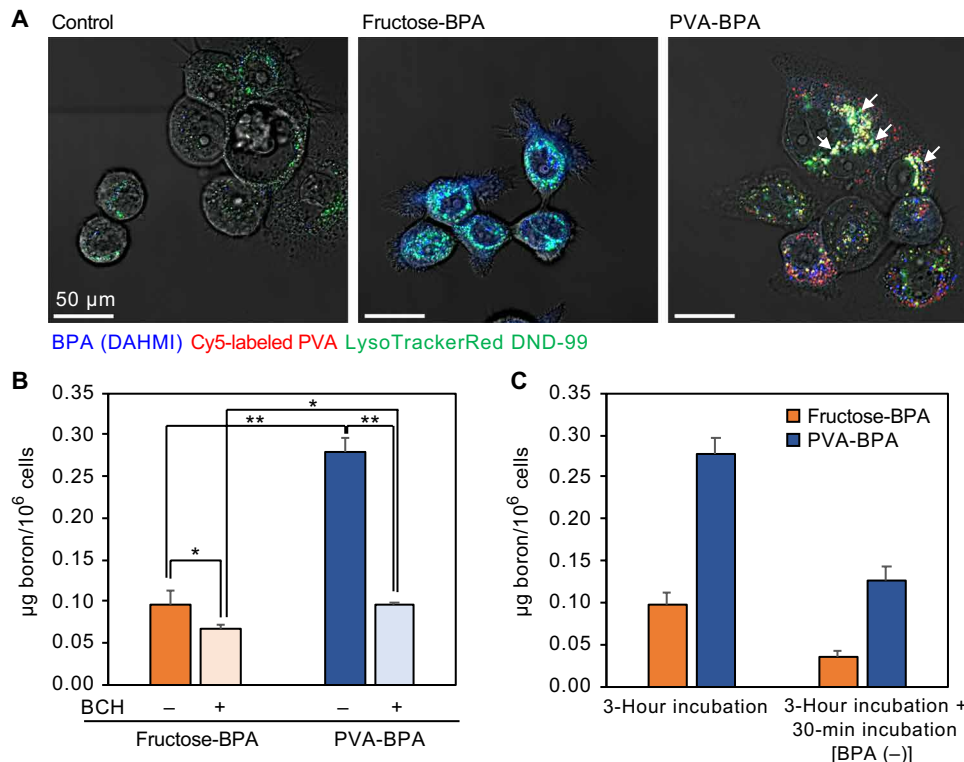


Fig. 2. Cellular uptake and subcellular localization. (A) Confocal laser scanning microscopic images of BxPC-3 cells incubated with fructose-BPA and Cy5-labeled PVA-BPA. BPA and endo-/lysosomes were labeled using DAHMI and LysoTracker Red DND-99, respectively. Control cells were treated with DAHMI and LysoTracker Red DND-99. BPA (DAHMI), Cy5-labeled PVA, and endo-/lysosomes (LysoTracker Red DND-99) are shown in blue, red, and green, respectively. White arrows indicate representative colocalization of DAHMI, Cy5, and LysoTracker Red DND-99. (B) Cellular uptake of BPA. BxPC-3 cells were incubated with BPA for 3 hours without/with system L inhibitor (BCH). The results are expressed as means \pm SD ($n = 3$). * $P < 0.05$ and ** $P < 0.001$ (Neuman-Keuls test). (C) Intracellular retention of BPA. The cells were incubated with BPA for 3 hours without/with additional incubation in fresh medium without BPA. The results without the additional incubation are the same with those shown in (B). The results are expressed as means \pm SD ($n = 3$).

endo-/lysosomal environment might cleave the boronate esters of PVA-BPA, and the liberated BPA may react with DAHMI, thereby emitting strong fluorescence.

Cellular uptake

Cellular uptake was examined by quantifying intracellular boron using inductively coupled plasma mass spectrometry (ICP-MS) both with and without an inhibitor for system L amino acid transporters, 2-amino-2-norbornanecarboxylic acid (BCH), to evaluate the specificity of PVA-BPA to LAT1 (Fig. 2B). In the absence of BCH, PVA-BPA exhibited 2.9 times higher cellular uptake compared with fructose-BPA. It is noteworthy that addition of BCH significantly reduced the cellular uptake of both fructose-BPA and PVA-BPA, indicating that PVA-BPA can be recognized by system L amino acid transporters including LAT1. These results suggest that PVA-BPA might be internalized into cells via LAT1-mediated endocytosis, which may facilitate the cellular internalization of BPA.

Next, intracellular retention was investigated to elucidate the effect of alteration of subcellular localization on the metabolism of BPA. The cells were allowed to take up the samples for 3 hours and were subsequently incubated in the fresh medium without BPA. As shown in Fig. 2C, fructose-BPA critically decreased the intracellular boron amount, which is in line with a previous study reporting that intracellular BPA was exchanged with extracellular amino acids (5). PVA-BPA also exhibited a lower amount of intracellular boron after

the additional incubation; however, compared with fructose-BPA, PVA-BPA exhibited 3.6 times higher intracellular boron concentration. Given that the intracellular boron concentration of PVA-BPA was 2.9 times higher than that of fructose-BPA before the additional incubation, the efflux of PVA-BPA should be more moderate than that of fructose-PVA. The efflux of boron observed in PVA-BPA-treated cells might be caused by several mechanisms. First, the exchange of BPA in the cytosol with the extracellular amino acids should contribute to the efflux as observed in fructose-BPA-treated cells, as CLSM observation indicated that some of the BPA not involved in the PVA-BPA complex formation was localized in the cytosol. The second possible mechanism involves the antiport activity of LAT1 on endosomal membranes. BPA in the endo-/lysosomes may be transferred into the cytosol through LAT1, leading to the efflux by exchange transport on the cell membrane. However, these steps are expected to slow the untoward efflux of intracellular BPA. The third possibility is exocytosis, because LAT1 involved in the endocytosis might be recycled to the cell membrane, leading to the export of PVA-BPA outside the cell. The fourth possibility is degradation of BPA. BPA in the cell might be metabolized into boric acids, which may then diffuse to the extracellular region (17). Despite the efflux of intracellular BPA in PVA-BPA-treated cells, the final intracellular boron concentration was maintained at a higher level compared with fructose-BPA. To summarize, PVA-BPA was internalized into cells through LAT1-mediated endocytosis, and the

localization of BPA in endo-/lysosomes slowed the efflux of intracellular BPA.

Biodistribution

To examine the potential of PVA-BPA for in vivo application, we first evaluated tumor accumulation. Fructose-BPA or PVA-BPA was intravenously injected to a BALB/c nude mouse bearing a subcutaneous BxPC-3 tumor, and the amount of intratumoral boron was quantified using ICP-MS (Fig. 3A). Fructose-BPA exhibited high tumor accumulation at 1 and 3 hours after injection, reaching 3.9% dose/g tumor. However, the tumor accumulation level gradually decreased with time, showing 1.2% dose/g tumor at 6 hours after injection. This decrease should be due to the untoward efflux of intracellular BPA. By contrast, PVA-BPA revealed significantly higher accumulation and longer retention in the tumor, achieving 6.4, 9.0, and 6.8% dose/g tumor 1, 3, and 6 hours after injection, respectively.

Similar tumor accumulation was also observed in a subcutaneous CT26 tumor model in a BALB/c mouse (Fig. 3B). Fructose-BPA attained high tumor accumulation at 6.6% dose/g tumor 1 hour after injection, and the level decreased to 2.2% dose/g tumor within 6 hours. Meanwhile, PVA-BPA maintained a high amount of intratumoral boron (>6.9% dose/g tumor) for 6 hours. It should be noted that the efficient accumulation and the prolonged retention of PVA-BPA within the tumor cannot be explained by the enhanced permeability and retention effect (EPR effect) (18). As shown in Fig. 3 (C to E), PVA-BPA could be excreted from the kidney similarly to fructose-BPA. Because the molecular weight of PVA should be subject to glomerular filtration (19), PVA-BPA was quickly cleared from blood circulation and normal organs. PVA-BPA eventually exhibited the high boron concentration ratios of tumor to blood (T/B ratios) comparable to those of fructose-BPA (fig. S7). Considering that the EPR effect is caused by augmented permeability of tumor vasculature and

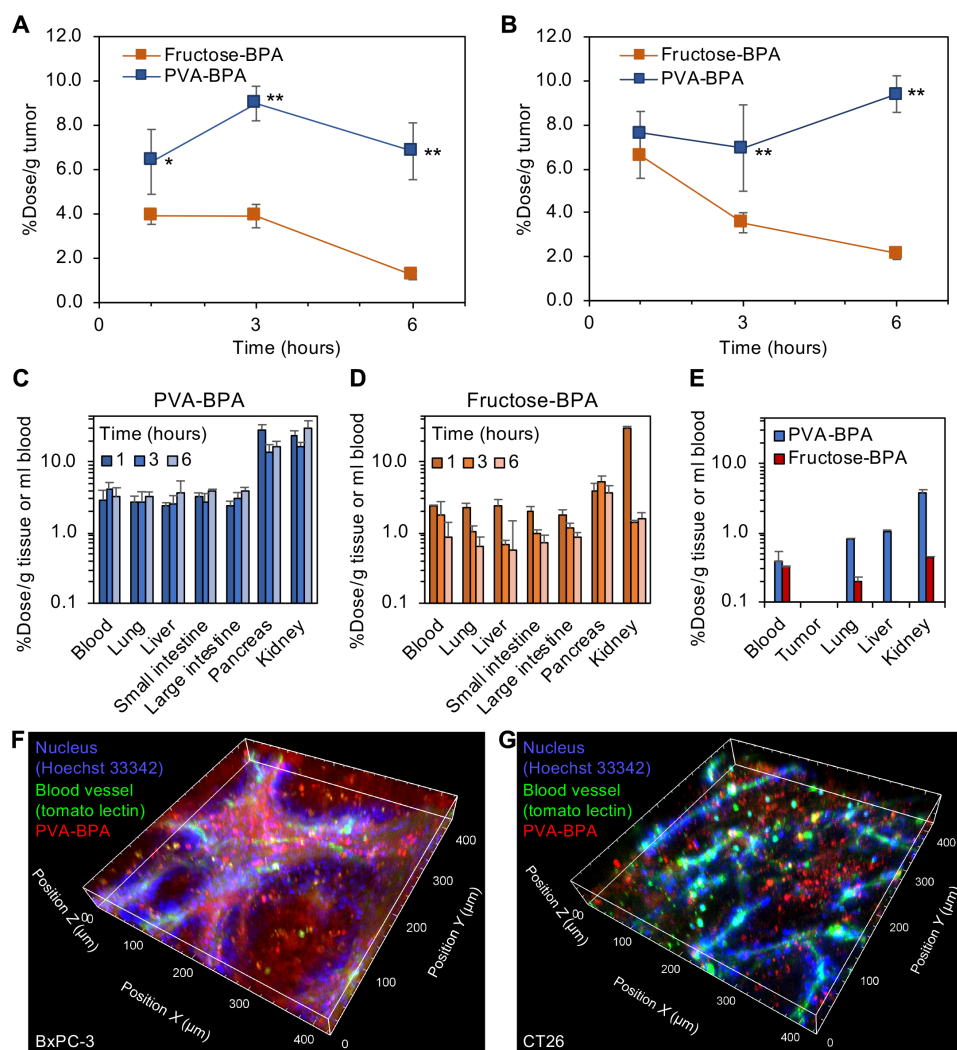


Fig. 3. Biodistribution and intratumoral distribution. (A) Tumor accumulation within a subcutaneous hypovascular BxPC-3 tumor in a BALB/c nude mouse. The results are expressed as means \pm SD ($n = 4$). * $P < 0.01$ and ** $P < 0.001$ (Tukey post hoc test). (B) Tumor accumulation within a subcutaneous hypervascular CT26 tumor in a BALB/c mouse. The results are expressed as means \pm SD ($n = 4$). ** $P < 0.001$ (Tukey post hoc test). (C and D) Distribution to normal organs of (C) PVA-BPA and (D) fructose-BPA. The results are expressed as means \pm SD ($n = 4$). (E) Distribution to normal organs 24 hours after administration. The results are expressed as means \pm SD ($n = 3$). (F and G) Intratumoral distribution of Cy5-labeled PVA-BPA in (F) a BxPC-3 tumor model and (G) a CT26 tumor model. Nuclei and blood vessels were labeled with intravenously injected Hoechst 33342- and DyLight 488-conjugated tomato lectin, respectively.

is generally observed with drugs exhibiting prolonged blood retention to increase opportunities to extravasate from vasculature into tumor tissue, the tumor accumulation and intratumoral retention of PVA-BPA should be achieved by the active targeting of LAT1 and subsequent endocytosis delaying the efflux from the target cells as observed in the *in vitro* study (Fig. 2). This explanation for the active targeting can be supported by the augmented accumulation within the pancreas (Fig. 3C) because the murine pancreas expresses LAT1 (20), while LAT1 expression in the human pancreas was reported to be undetectable (21). To get more insight about the tumor accumulation, we prepared a complex of PVA and ^{19}F -BPA (PVA- ^{19}F -BPA) and evaluated its tumor accumulation (fig. S8). PVA- ^{19}F -BPA also exhibited prolonged intratumoral retention compared with fructose- ^{19}F -BPA. These results strongly suggest that complex formation with PVA can improve tumor accumulation and retention of BPA and its derivatives.

Intratumoral distribution

Since homogeneous distribution of boron is critical for successful treatment, we assessed intratumoral distribution of PVA-BPA. Cy5-PVA-BPA was injected to the BxPC-3 and CT26 tumor models through the tail vein, and nuclei and blood vessels were labeled with intravenously injected Hoechst 33342- and DyLight 488-conjugated tomato lectin, respectively. The tumor was observed using CLSM 3 hours after the injection of Cy5-PVA-BPA (Fig. 3, F and G). Hoechst 33342, which was used for nucleus staining, could not efficiently reach the deep part (the region away from the blood vessels), and its strong fluorescence was observed near the blood vessels. It is reported that membrane-permeant Hoechst 33342 shows low interstitial penetration, possibly because cellular uptake is faster than diffusion in a tumor (22). By contrast, Cy5-PVA-BPA exhibited accumulation even in the deep part where Hoechst 33342 could not be delivered in both BxPC-3 and CT26 tumors. Particularly in the hypervascular CT26 tumor, Cy5-PVA-BPA nearly homogeneously distributed, which is a prerequisite for the complete treatment by BNCT. On the other hand, in the hypovascular BxPC-3 tumor having rich stroma, strong Cy5 fluorescence was observed near the blood vessels, which is consistent with a previous study reporting that the stroma should disturb drug penetration (23). However, as previously mentioned, considerable accumulation

of Cy5-PVA-BPA could also be observed within the deep part of the tumor. Thus, PVA-BPA is expected to have the potential to deliver a strong therapeutic effect even in the hypovascular tumor model.

Neutron capture therapy using PVA-BPA

The therapeutic potential of PVA-BPA was examined using a subcutaneous BxPC-3 tumor model in a mouse. We intravenously injected fructose-BPA or PVA-BPA to the mouse (10 mg BPA per mouse) and irradiated epi-/thermal neutrons to the tumor for 50 min 3 hours after injection (Fig. 4). Both fructose-BPA and PVA-BPA appreciably suppressed tumor growth, and PVA-BPA showed significantly higher antitumor activity (Fig. 4A). It is worthwhile to note that some of the fructose-BPA-treated tumors exhibited obvious regrowth (mouse1 to mouse4 in Fig. 4B), while PVA-BPA suppressed tumor growth for a longer period of time than fructose-BPA (Fig. 4C). This enhanced antitumor activity of PVA-BPA is consistent with the observed augmented accumulation and prolonged retention in the tumor (Fig. 3A), as well as the efficient intratumoral penetration (Fig. 3F).

We also evaluated antitumor activity in a subcutaneous CT26 tumor model (Fig. 5). In a similar way to the aforementioned experiment, fructose-BPA or PVA-BPA was intravenously injected to the mouse, and the tumor was irradiated with epi-/thermal neutrons for 50 min 3 or 6 hours after injection. As shown in Fig. 5A, without neutron irradiation, neither fructose-BPA nor PVA-BPA induced antitumor activity; however, with the irradiation, they accomplished significant suppression without apparent side effect (Fig. 5C). Similar to the study in the BxPC-3 tumor model (Fig. 4), PVA-BPA exhibited a significantly higher antitumor effect (Fig. 5B). The strong antitumor effect of PVA-BPA with 3-hour interval was also confirmed by histological analysis of the tumor after treatment (Fig. 5, D and E). While the fructose-BPA-treated tumor still had living tumor cells as characterized with large nuclei, the PVA-BPA-treated tumor revealed shrinkage of nuclei, indicating the death of tumor cells. These results suggest the importance of intratumoral retention of BPA in NCT.

DISCUSSION

In this study, to control metabolism of BPA by modulating its subcellular localization, we used PVA for complex formation with BPA

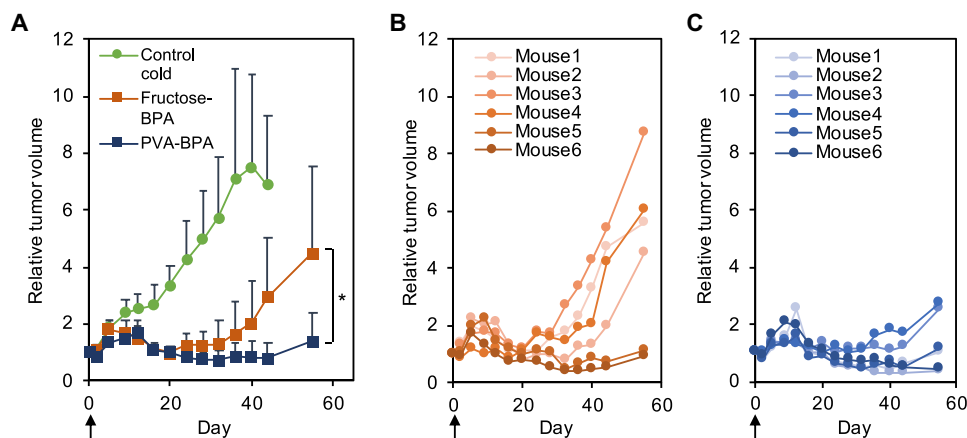


Fig. 4. Antitumor effect in a subcutaneous hypovascular BxPC-3 tumor model. (A) Tumor growth curves. The indicated samples were intravenously injected, and the tumors were irradiated with epi-/thermal neutrons 3 hours after injection on day 0. The results are expressed as means \pm SD ($n = 8$ for control; $n = 6$ for fructose-BPA and PVA-BPA). $*P < 0.05$ (one-way Student's *t* test). (B and C) Individual tumor growth treated with (B) fructose-BPA and (C) PVA-BPA.

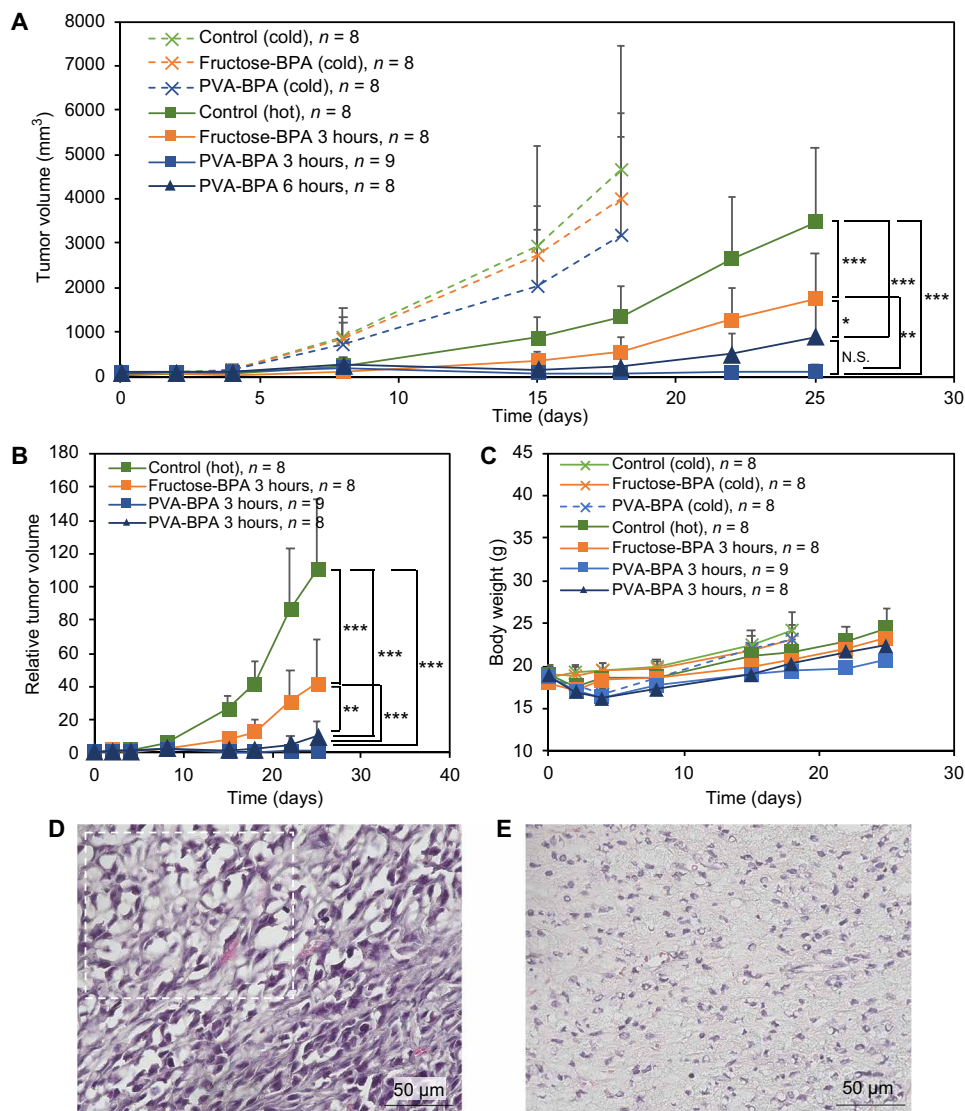


Fig. 5. Antitumor effect in a subcutaneous hypervascular CT26 tumor model. (A and B) Tumor growth curves. The indicated samples were intravenously injected, and the tumors were irradiated with epi-/thermal neutrons 3 or 6 hours after injection on day 1. The results are expressed as means \pm SD. * P < 0.05, ** P < 0.00001, and *** P < 0.0000001 (Bonferroni method) in (A). N.S., not significant. ** P < 0.0001 and *** P < 0.000001 (Bonferroni method) in (B). (C) Body weight. The results are expressed as means \pm SD. (D and E) Histology (hematoxylin and eosin) of tumors treated by BNCT with (D) fructose-BPA and (E) PVA-BPA (3-hour interval). The tumors were collected 25 days after the treatment. The dashed rectangle in (D) indicates a representative damaged region characterized by shrinkage of nuclei.

because of the extremely high dose of BPA compared with the other therapeutic drugs. In clinical BNCT, intratumoral boron concentration should be more than 25 parts per million to attain effective therapeutic outcome. To achieve this high intratumoral boron concentration, BPA is injected to patients at a dose of 500 mg/kg. Thus, the polymer that forms a complex with BPA should be also injected at a likewise high dose and should be considerably biocompatible. In addition, to minimize the dose of the polymer, it should have a simple chemical structure. In this regard, PVA has been widely studied as a biocompatible polymer (24, 25), and it also has the simplest chemical structure necessary to form the boronate ester. These characteristics made PVA suitable for the purpose of this study.

Clinical BNCT prefers high T/B ratios or boron concentration ratios of tumor to normal organs (T/N ratios) to avoid untoward radiation damage to normal organs. Generally, drug delivery systems

showing long circulation in the bloodstream have difficulty in achieving the high T/B ratio. Hence, we used PVA with M_n < 10,000 to induce quick clearance of BPA from the body. As shown in Fig. 3C and fig. S7, PVA-BPA was quickly cleared from the body, and the T/N and T/B ratios were comparable to those of fructose-BPA. Likely owing to the quick clearance and biocompatibility of PVA, PVA-BPA did not show apparent severe toxicity. Despite the quick clearance from the blood, PVA-BPA accomplished efficient tumor accumulation as we conjugated BPA molecules with PVA through boronate esters to expose phenylalanine structures of BPA molecules to target LAT1. We recently reported that polymers having multiple glutamines have a strong affinity to dense ASCT2 transporters (glutamine transporters) that are overexpressed on tumor cells through the multivalent effect and can be efficiently taken up by the cells through ASCT2-mediated endocytosis (26). Recent studies by other groups also demonstrated

transporter-targeted delivery of nanoparticles and their internalization through transporter-mediated endocytosis (27). The cellular uptake mechanism of PVA-BPA may be similar to these systems because our PVA-BPA could be internalized into tumor cells through LAT1-mediated endocytosis, thereby enhancing cellular uptake (Fig. 2, A and B). Note that the multivalent effect of PVA-BPA was not clarified in this study. However, even if PVA-BPA could not induce multivalent interaction with LAT1, PVA-BPA should still have the potential to induce LAT1-mediated endocytosis, as it was previously reported that introduction of a phenylalanine structure to a polymer could facilitate the interaction of the polymer with LAT1, resulting in LAT1-mediated endocytosis (28). According to previous studies (27, 28), physicochemical properties including hydrophilicity of the ligand (transporter substrate)-conjugated polymer and ligand density may also be the critical parameters determining the interaction with the targeted transporter and subsequent cellular uptake. Elucidation of these parameters may be important for the translation of PVA-BPA to a clinical setting, and we are now developing a series of polymer-BPA conjugates having various physicochemical properties. These topics will be discussed in our future work.

Through the LAT1-mediated endocytosis, PVA-BPA was localized in the endo-/lysosomes and accomplished prolonged retention in the tumor (Figs. 2C and 3, A and B), thereby enhancing the BNCT effect (Figs. 4 and 5). However, the *in vitro* analysis (Fig. 2C) indicated obvious decrease in intracellular BPA, which appears to be inconsistent with the drastically prolonged tumor retention observed in the *in vivo* study (Fig. 3, A and B). This discrepancy between *in vitro* and *in vivo* may be explained by the extreme condition of the *in vitro* experiment, in which BPA was completely removed during the additional incubation, allowing the cells to efflux BPA. In actual *in vivo* studies, the extracellular region contains BPA, which should also be taken up by tumor cells and compensate for the exported BPA. Also, the slightly prolonged retention in the blood (Fig. 3C) might contribute to the intratumoral retention of PVA-BPA. PVA-BPA in the bloodstream might supply BPA to the tumor even during irradiation of thermal neutrons, leading to the enhanced BNCT effect (Figs. 4 and 5). Nevertheless, we used PVA with the molecular weight (M_n) < 10,000, permitting the quick renal clearance. PVA-BPA eventually exhibited the high T/B ratios comparable to fructose-BPA (fig. S7).

In addition to the above-described tumor retention, controlling intratumoral distribution of ^{10}B is an important factor in determining the therapeutic outcome of BNCT, as the range of α particles and Li recoil nuclei is limited to 10 μm . Nakamura *et al.* reported that liposomal boron clusters enhanced tumor accumulation, but the heterogeneous intratumoral distribution should compromise the therapeutic efficacy (29). In addition, we previously reported that size of drug delivery systems critically affects their intratumoral distribution; nanoparticles with a diameter of 70 nm could not penetrate into the deep regions of a BxPC-3 tumor characterized by rich stroma and hypovascularity, while those with a diameter of 30 nm exhibited efficient penetration (23, 30). Because the molecular weight (M_n) of our PVA was <10,000, it is expected that PVA-BPA can efficiently penetrate into the deep regions. Cy5-PVA-BPA reached the deep part of the tumor where Hoechst 33342 could not stain the nuclei (Fig. 3F). Besides, the efficient penetration might be partly due to the extremely high dose of BPA. In the biodistribution study (Fig. 3, A and B), PVA-BPA exhibited >6% dose/g tumor, which corresponds to >2 mM of BPA in the tumor. According to the previous study (6),

LAT1 should be saturated at this concentration. Thus, although PVA-BPA can be efficiently taken up by the tumor cells through LAT1-mediated endocytosis (Fig. 2B), there should be a considerable amount of PVA-BPA in the extracellular region. Such PVA-BPA may not stay near blood vessels but penetrate into the deep region.

Note that the high dose of BPA may also contribute to the stable complex formation of PVA-BPA. One may wonder about the dissociation of PVA-BPA in the blood containing abundant glucose because the apparent binding constant between PVA and BPA at pH 7.4 was 0.8 times that between glucose and BPA, which was quantified by fluorescence analysis with Alizarin red S (31). However, the BPA concentration in the blood should be much higher (approximately 20 mM) than the glucose concentration (roughly 5 mM) if all the injected BPA was mixed with the blood in the body. Most BPA molecules should be still conjugated to PVA immediately after injection. Meanwhile, it is well known that lowered pH decreases binding constants between boronic acids and diols. Slightly acidic tumorous pH may facilitate the dissociation of BPA from PVA-BPA. Thus, the intratumoral distribution of BPA might be different from the observed Cy5-fluorescent image, but the dissociated BPA is expected to diffuse into the deep region. Since such analysis would be helpful to estimate its therapeutic effect with irradiation of thermal neutrons and important for the clinical translation of PVA-BPA, we plan to analyze the distribution of the boron of PVA-BPA using autoradiography and may report it in the future study.

Efficient intratumoral penetration, however, does not always guarantee a complete cure in BNCT using BPA. The therapeutic effect of BPA has been compromised not only by the clearance from the tumor but also by quiescent tumor cells showing lower cellular uptake of BPA compared with other cells (32, 33). This may partly account for the regrowth of the fructose-BPA-treated CT26 tumors (Fig. 5, A, B, and D). By contrast, PVA-BPA exhibited enhanced antitumor activity (Figs. 4 and 5), and histological analysis indicated complete cure in some CT26 tumor models (Fig. 5E). It is likely that PVA-BPA altered the cellular uptake pathway and might increase the uptake efficiency even in the quiescent cells. This possibility will be further investigated in our future work because such analysis into boron distribution with simulation of radiation dose would be necessary for rationale prediction of the radiobiological effect of BNCT (34).

With respect to the clinical prediction of the BNCT effect, positron emission tomography (PET) using ^{18}F -BPA is a powerful tool used as companion diagnostics. Because the half-life of ^{18}F is only 1.8 hours, it is generally difficult to conjugate or encapsulate ^{18}F -BPA within nanoparticles such as liposomes and micelles that require many steps for manufacture. On the other hand, PVA- ^{19}F -BPA can be easily and promptly prepared in aqueous solution, and PVA- ^{19}F -BPA demonstrated enhanced tumor accumulation and retention (fig. S8). Thus, the concept of this study can be extended to the companion diagnostics using PET with ^{18}F -BPA. PET with PVA- ^{18}F -BPA would clarify the biodistribution in patients, which cannot be precisely expected from experiments using animals. For example, as aforementioned, a murine pancreas expresses high level of LAT1 unlike that of a human (20, 21). The PET technique should overcome the discrepancy of pharmacokinetics, which is caused by difference between species. These theranostic benefits provided by the simple preparation of PVA-BPA would permit its smooth clinical application.

Although PVA-BPA benefits from the aforementioned advantages, further investigation is necessary before its expansion to the clinical setting. First, the molecular weight of PVA should be optimized. PVA

($M_n = 9500$) accomplished prolonged tumor retention, but increasing or decreasing the molecular weight may affect the therapeutic potential and side effects. As a previous study described (19), the molecular weight of PVA critically affects its biodistribution. A higher molecular weight of PVA should lead to its longer retention in the blood as well as more efficient tumor accumulation via the EPR effect. However, as discussed above, long blood circulation lowers the T/B ratio, which is not preferable in BNCT. Thus, it is necessary to elucidate the optimal molecular weight of PVA-BPA that permits enhanced tumor accumulation and retention with quick clearance from the blood and normal organs. Second, possible side effects should be further investigated even though PVA has been clinically used and its excellent biocompatibility has been widely reported (24, 25). Since one of the most important advantages of BNCT is its minimal invasiveness, even minute effects on normal organs must not be ignored, and these issues are currently being studied further.

MATERIALS AND METHODS

Materials

BPA (^{10}B) was purchased from Katchem spol s.r.o. (Praha, the Czech Republic). ^{19}F -BPA was obtained from Fluorotech LLC (Gainesville, FL). Vinyl acetate (VAc), D-fructose, benzene, tetrahydrofuran (THF), Alizarin red S, 10% formalin neutral buffer solution, nitric acid, hydrochloric acid (HCl), and sodium hydroxide (NaOH) were purchased from Wako Pure Chemical Industries Ltd. (Osaka, Japan). The reagents for hematoxylin and eosin stain were purchased from Muto Pure Chemicals Co. Ltd. (Tokyo, Japan). BPA (^{11}B), 2,2'-azobis(2-methylpropionitrile) (AIBN), cyanomethyl methyl(phenyl) carbamodithioate (CTA), BCH, penicillin-streptomycin solution, and trypsin-EDTA solution were purchased from Sigma-Aldrich (St. Louis, MO). 4-Diethylaminosalicylaldehyde and methylamine were purchased from Tokyo Chemical Industry Co. Ltd. (Tokyo, Japan). Hexane and ethyl acetate were purchased from Kanto Chemical Co. Inc. (Tokyo, Japan). Methanol (MeOH), dimethyl sulfoxide (DMSO), Dulbecco's phosphate-buffered saline (D-PBS), and sodium chloride were obtained from Nacalai Tesque Inc. (Kyoto, Japan). LysoTracker Red DND-99 and Hoechst 33342 were purchased from Thermo Fisher Scientific (Waltham, MA). Cy5 NHS ester was obtained from Lumiprobe Corporation (Hunt Valley, MD). PD-10 column was purchased from GE Healthcare Japan Corporation (Tokyo, Japan). Cell culture dishes and glass-base dishes were obtained from AGC Techno Glass Co. Ltd. (Shizuoka, Japan). PTFE (polytetrafluoroethylene) syringe filter (0.5 μm) was obtained from Advantec (Tokyo, Japan). Polyvinylidene difluoride syringe filter (0.45 μm) was obtained from Merck KGaA (Darmstadt, Germany). DyLight 488-labeled *Lycopersicon esculentum* (tomato) lectin was purchased from Vector Laboratories (Burlingame, CA). O.C.T. compound was obtained from Sakura Finetek Japan Co. Ltd. (Tokyo, Japan). Fetal bovine serum (FBS) was obtained from Biosera (Kansas City, MO). Entellan new was purchased from Merck KGaA.

Cells and animals

BxPC-3 human pancreatic adenocarcinoma cells and CT26 murine colon cancer cells were purchased from the American Type Culture Collection (Manassas, VA), and RPMI 1640 medium containing 10% FBS and 1% penicillin-streptomycin was used as culture medium. Cells were cultured in a humidified atmosphere containing 5% CO_2 at 37°C. Animals were obtained from Charles River Laboratories

Japan Inc. (Yokohama, Japan). All the animal experiments were approved by the Animal Care and Use Committee of Tokyo Institute of Technology and the Animal Care and Use Committee of Kyoto University. The experiments were performed in accordance with the Guidelines for the Care and Use of Laboratory Animals as stated by Tokyo Institute of Technology and the Guidelines for the Care and Use of Laboratory Animals as stated by Kyoto University.

Synthesis of PVAc

PVAc was synthesized using RAFT polymerization, following a previous report (35). Typically, AIBN (0.0174 mmol), CTA (0.0174 mmol), and VAc (34.8 mmol) were mixed in a flask under Ar atmosphere. After degassing by freeze-pump-thaw cycles, the mixture was stirred at 60°C. Following 24-hour reaction, the mixture was dialyzed against THF and freeze dried with benzene. PVAc was obtained as an orange solid. Molecular weight distribution and degree of polymerization were determined by GPC [column: TSKgel SuperAW3000, SuperAW4000, and SuperAWL-guard column (Tosoh Corporation, Yamaguchi, Japan); eluent: NMP (*N*-methyl-2-pyrrolidone) containing 50 mM lithium bromide; flow rate: 0.3 ml/min; detector: refractive index; temperature: 40°C] (fig. S2) and ^1H NMR (Bruker Avance III, 400 MHz, Bruker BioSpin, Billerica, MA) (fig. S3).

Synthesis of PVA

PVA was obtained by saponification of PVAc. Briefly, PVAc (0.062 mmol) was dissolved in 30 ml of MeOH in a flask, and NaOH (5 equivalent to VAc units) and water were added to the solution. The mixture was stirred at 60°C for 24 hours and dialyzed against water. After filtering the obtained solution using a syringe filter (0.45 μm), PVA was obtained as a white solid by lyophilization. The obtained PVA was characterized by GPC [column: Superdex 200 Increase (GE Health Care Japan, Tokyo, Japan); eluent: buffer containing 10 mM phosphate and 140 mM NaCl (pH 7.4); flow rate: 0.75 ml/min; temperature: room temperature] (fig. S4) and ^1H NMR (Bruker Avance III, 400 MHz) (fig. S5).

Synthesis of Cy5-PVA

To label PVA with Cy5, PVA was dissolved in DMSO, and Cy5-NHS (1.2 equivalent to PVA) was added to the solution and stirred for 3 hours at room temperature. After the reaction, the solution was dialyzed against water, and free Cy5 was removed using PD-10 column.

Synthesis of DAHMI

Following a previous study (15), DAHMI for detecting BPA was synthesized by the reaction of 4-diethylaminosalicylaldehyde and methylamine in methanol with reflux for 24 hours, followed by the concentration in vacuo and subsequent purification by flash SiO_2 column chromatography (eluent: hexane/ethyl acetate).

^{11}B NMR analysis

Fructose-BPA solution was prepared by dissolving fructose (574 mM) and BPA (191 mM) in aqueous buffer solution containing 10 mM phosphate and 140 mM NaCl (pH 9.5). PVA-BPA solution was also prepared by dissolving PVA (574 mM of diol unit) and BPA (191 mM) in the buffer. BPA solution was prepared just by dissolving BPA in the buffer without solubilizer. Each sample was mixed with D_2O ($v/v = 9/1$), and ^{11}B NMR was measured using Bruker Avance III HD 500 (500 MHz, Bruker BioSpin).

Quantification of apparent complex formation constant between PVA and BPA

Apparent complex formation constant was quantified using Alizarin red S following the protocol reported in a previous study (31). Fluorescence of Alizarin red S–BPA complexes was measured with glucose or PVA at variable concentrations using a fluorophotometer (FP-8300, JASCO Corporation, Tokyo, Japan). The apparent complex formation constant was calculated with the assumption that a glucose molecule should form a complex with a BPA molecule, while a diol unit in PVA should form a boronate ester.

CLSM observation of subcellular localization

BxPC-3 cells were seeded on a glass-base dish (5×10^4 cells per dish) and incubated for 24 hours. After removing the medium, the cells were incubated in medium [D-PBS/RPMI = 1/4 (v/v)] containing fructose-BPA (fructose: 290 μ M, BPA: 110 μ M) or Cy5-PVA-BPA (diol unit in Cy5-PVA: 340 μ M, BPA: 110 μ M) for 30 min. The cells were then incubated in D-PBS containing 20 μ M DAHMI and 50 nM LysoTracker Red DND-99 for 30 min, followed by washing with D-PBS thrice. The cells in D-PBS were observed using CLSM (LSM710, Carl Zeiss AG, Oberkochen, Germany).

Cellular uptake

To evaluate cellular uptake, BxPC-3 cells were seeded on a dish (5×10^6 cells per dish) and incubated for 24 hours. After removing the medium, the cells were incubated in the medium [D-PBS/culture medium = 1/4 (v/v)] containing fructose-BPA (fructose: 7.8 mM, BPA: 3.0 mM) or PVA-BPA (diol unit in PVA: 3.0 mM, BPA: 3.0 mM) with/without BCH (20 mM) for 3 hours. The cells were then washed with D-PBS and detached by incubation in 1 ml of trypsin/EDTA solution. The cell suspension was mixed with 9 ml of culture medium, and the cells were collected by centrifugation. After counting the number of cells, they were lysed in 1 ml of 70% nitric acid and ashed by heating the lysate at 90°C. The ashed sample was diluted with water, and the volume was adjusted to 10 ml, followed by filtration using a syringe filter (0.5 μ m). The amount of boron in the filtered samples was quantified using ICP-MS (Agilent 7900 ICP-MS, Agilent Technologies Inc., Santa Clara, CA).

For the assessment of intracellular boron retention, the cells were incubated with fructose-BPA or PVA-BPA without BCH for 3 hours as described above. The cells were then incubated in fresh medium without BPA for 30 min to allow cells to export intracellular boron, followed by collection with trypsin/EDTA. The subsequent procedures were the same with the aforementioned protocols.

Biodistribution

A subcutaneous BxPC-3 tumor model was prepared by subcutaneous inoculation of BxPC-3 cells into a BALB/c nude mouse (5×10^6 cells per mouse). A subcutaneous CT26 tumor model was also prepared by subcutaneously inoculating CT26 cells into a BALB/c mouse (2×10^5 cells per mouse). After the tumor size reached approximately 200 mm³, fructose-BPA (molar ratio of fructose to BPA = 3, pH 9.2 to 9.5) or PVA-BPA (molar ratio of diol unit in PVA to BPA = 3, weight ratio of PVA to BPA = 1.3, pH 9.2 to 9.5) was intravenously injected to the mouse (BPA 8 mg per mouse). The mice were euthanized 1, 3, or 6 hours after injection, and blood was obtained from the inferior vena cava and heparinized, followed by collection of tumors and organs. The collected samples were soaked in 1 ml of 70% nitric acid and ashed at 90°C. The ashed samples were diluted with water, and

the volume was adjusted to 10 ml. After filtering the samples with a syringe filter (0.5 μ m), the amount of boron in the samples was quantified using ICP-MS (Agilent 7900 ICP-MS).

In the evaluation of biodistribution of ¹⁹F-BPA, fructose-¹⁹F-BPA (molar ratio of fructose to ¹⁹F-BPA = 3.2, pH 9.5) or PVA-¹⁹F-BPA (molar ratio of diol unit in PVA to ¹⁹F-BPA = 3.2, weight ratio of PVA to ¹⁹F-BPA = 1.3, pH 9.5) was intravenously injected to the mouse bearing a subcutaneous CT26 tumor (¹⁹F-BPA 8 mg per mouse). The tumors were collected 1 or 6 hours after injection and processed in the same procedures with the aforementioned methods for the analysis using ICP-MS.

Intratumoral distribution

Tumor models were prepared using the same procedures described in the section on “Biodistribution.” After the tumor size reached approximately 200 mm³, Cy5-PVA-BPA (molar ratio of diol unit in Cy5-PVA to BPA = 3, weight ratio of Cy5-PVA to BPA = 1.3, pH 9.2 to 9.5) was intravenously injected to the mouse (BPA 8 mg per mouse). The mouse was then injected with Hoechst 33342 (250 μ g per mouse) and DyLight 488–labeled tomato lectin (25 μ g per mouse) 2.5 hours after injection of Cy5-PVA-BPA to visualize nuclei and blood vessels, respectively. After 30 min, the mouse was euthanized, and the tumor was collected and cut in half. The cut tumor was put on a glass-base dish, and the cross section was observed under a humidified atmosphere using LSM710. Three-dimensional imaging was constructed using the Imaris software (Bitplane AG, Zurich, Switzerland).

Neutron capture therapy to BxPC-3 tumor models

BxPC-3 cells (5×10^6 cells per mouse) were subcutaneously inoculated into the right thighs of BALB/c nude mice. The tumors were allowed to grow for ~2 months. The mouse was injected with fructose-BPA (molar ratio of fructose to BPA = 3, pH 9.2) or PVA-BPA (molar ratio of diol unit in PVA to BPA = 3, weight ratio of PVA to BPA = 1.3, pH 9.2) at a dose of 10 mg of BPA per mouse. The mice were placed in acrylic holders, which were secured on a 5-mm-thick thermoplastic plate that contained 40 weight % (wt %) of ⁶LiF (96% ⁶Li) to block thermal neutrons and had a circular hole in the center. The thigh containing the tumor was stretched over the hole, and the tumor was irradiated with epi-/thermal neutrons for 50 min (fluence: 9.9×10^{11} to 4.5×10^{12} neutrons/cm²) 3 hours after the injection. The tumor size was measured by a caliper, and the tumor volume (*V*) was calculated using the following equation: $V = ab^2/2$, where *a* and *b* are the major and minor axes, respectively.

Neutron capture therapy to CT26 tumor models

CT26 cells (2×10^5 cells per mouse) were subcutaneously inoculated into the right thighs of BALB/c mice. The tumors were allowed to grow for ~2 weeks. The mice were injected with fructose-BPA (molar ratio of fructose to BPA = 3, pH 9.5) or PVA-BPA (molar ratio of diol unit in PVA to BPA = 3, weight ratio of PVA to BPA = 1.3, pH 9.5) at a dose of 10 mg BPA per mouse. The mice were placed in acrylic holders, which were secured on a 5-mm-thick thermoplastic plate that contained 40 wt % of ⁶LiF (96% ⁶Li) to block thermal neutrons and had a circular hole in the center. The thigh containing the tumor was stretched over the hole, and the tumor was irradiated with epi-/thermal neutrons for 50 min (fluence: 1.1×10^{12} to 3.8×10^{12} neutrons/cm²) 3 or 6 hours after the injection. The tumor size was measured by a caliper, and the tumor volume (*V*) was calculated using the following

equation: $V = ab^2/2$, where a and b are the major and minor axes, respectively.

Histological analysis for CT26 tumors

BNCT-treated CT26 tumors were collected 25 days after the treatment and soaked in formalin solution. The fixed tumor was embedded in O.C.T. compound and frozen. Tissue sections with 4- μ m thickness were obtained using Leica CM3050S (Leica Biosystems, Wetzlar, Germany) and stained with hematoxylin and eosin. The tissue section was embedded in Entellan new and observed using a microscope (BZ-X710, Keyence Corporation, Osaka, Japan).

Statistical analysis

Statistical analysis was conducted using Student's t test, one-way analysis of variance (ANOVA), and two-way ANOVA with post hoc analysis. The P values less than 0.05 were considered statistically significant.

SUPPLEMENTARY MATERIALS

Supplementary material for this article is available at <http://advances.sciencemag.org/cgi/content/full/6/4/eaaz1722/DC1>

Fig. S1. Synthetic scheme of PVAc and PVA.

Fig. S2. GPC chart of PVAc.

Fig. S3. ^1H NMR spectrum of PVAc in DMSO- d_6 .

Fig. S4. GPC chart of PVA.

Fig. S5. ^1H NMR spectrum of PVA in DMSO- d_6 .

Fig. S6. ^{11}B NMR spectra of BPA, fructose-BPA, and PVA-BPA.

Fig. S7. T/B ratios in BxPC-3 and CT26 tumor models.

Fig. S8. Tumor accumulation of fructose- ^{19}F -BPA and PVA- ^{19}F -BPA in subcutaneous CT26 tumor models.

[View/request a protocol for this paper from Bio-protocol.](#)

REFERENCES AND NOTES

- R. L. Moss, Critical review, with an optimistic outlook, on Boron Neutron Capture Therapy (BNCT). *Appl. Radiat. Isot.* **88**, 2–11 (2014).
- M. J. Luderer, P. de la Puente, A. K. Azab, Advancements in tumor targeting strategies for boron neutron capture therapy. *Pharm. Res.* **32**, 2824–2836 (2015).
- T. Nomoto, N. Nishiyama, Design of drug delivery systems for physical energy-induced chemical surgery. *Biomaterials* **178**, 583–596 (2018).
- Y. Mishima, C. Honda, M. Ichihashi, H. Obara, J. Hiratsuka, H. Fukuda, H. Karashima, T. Kobayashi, K. Kanda, K. Yoshino, Treatment of malignant-melanoma by single thermal-neutron capture therapy with melanoma-seeking ^{10}B -compound. *Lancet* **2**, 388–389 (1989).
- A. Wittig, W. A. Sauerwein, J. A. Coderre, Mechanisms of transport of p -boronophenylalanine through the cell membrane in vitro. *Radiat. Res.* **153**, 173–180 (2000).
- P. Wongthai, K. Hagiwara, Y. Miyoshi, P. Wiriyasermkul, L. Wei, R. Ohgaki, I. Kato, K. Hamase, S. Nagamori, Y. Kanai, Boronophenylalanine, a boron delivery agent for boron neutron capture therapy, is transported by ATB $^{9+}$, LAT1 and LAT2. *Cancer Sci.* **106**, 279–286 (2015).
- K. Hanaoka, T. Watabe, S. Naka, Y. Kanai, H. Ikeda, G. Horitsugi, H. Kato, K. Isohashi, E. Shimosegawa, J. Hatazawa, FBPA PET in boron neutron capture therapy for cancer: Prediction of ^{10}B concentration in the tumor and normal tissue in a rat xenograft model. *EJNMMI Res.* **4**, 70 (2014).
- T. Watanabe, Y. Hattori, Y. Ohta, M. Ishimura, Y. Nakagawa, Y. Sanada, H. Tanaka, S. Fukutani, S. Masunaga, M. Hiraoka, K. Ono, M. Suzuki, M. Kirihata, Comparison of the pharmacokinetics between L-BPA and L-FBPA using the same administration dose and protocol: A validation study for the theranostic approach using ^{18}F -L-FBPA positron emission tomography in boron neutron capture therapy. *BMC Cancer* **16**, 859 (2016).
- L. Evangelista, G. Jori, D. Martini, G. Sotti, Boron neutron capture therapy and ^{18}F -labelled borophenylalanine positron emission tomography: A critical and clinical overview of the literature. *Appl. Radiat. Isot.* **74**, 91–101 (2013).
- Y. Mori, A. Suzuki, K. Yoshino, H. Kakihana, Complex-formation of p -boronophenylalanine with some monosaccharides. *Pigment Cell Res.* **2**, 273–277 (1989).
- H. Fukuda, C. Honda, N. Wadabayashi, T. Kobayashi, K. Yoshino, J. Hiratsuka, J. Takahashi, T. Akaizawa, Y. Abe, M. Ichihashi, Y. Mishima, Pharmacokinetics of 10B- p -boronophenylalanine in tumours, skin and blood of melanoma patients: A study of boron neutron capture therapy for malignant melanoma. *Melanoma Res.* **9**, 75–83 (1999).
- K. Ono, An analysis of the structure of the compound biological effectiveness factor. *J. Radiat. Res.* **57**, i83–i89 (2016).
- W. L. Yang, R. F. Barth, T. Y. Huo, G. W. Kabalka, A. L. Shaikh, S. A. Haider, S. Chandra, Effects of L-DOPA pre-loading on the uptake of boronophenylalanine using the F98 glioma and B16 melanoma models. *Appl. Radiat. Isot.* **88**, 69–73 (2014).
- B. Wingelhofer, K. Kreis, S. Mairinger, V. Muchitsch, J. Stanek, T. Wanek, O. Langer, C. Kuntner, Preloading with L-BPA, L-tyrosine and L-DOPA enhances the uptake of ^{18}F FBPA in human and mouse tumour cell lines. *Appl. Radiat. Isot.* **118**, 67–72 (2016).
- Y. Hattori, M. Ishimura, Y. Ohta, H. Takenaka, T. Watanabe, H. Tanaka, K. Ono, M. Kirihata, Detection of boronic acid derivatives in cells using a fluorescent sensor. *Org. Biomol. Chem.* **13**, 6927–6930 (2015).
- Y. Hattori, M. Ishimura, Y. Ohta, H. Takenaka, M. Kirihata, Visualization of boronic acid containing pharmaceuticals in live tumor cells using a fluorescent boronic acid sensor. *ACS Sens.* **1**, 1394–1397 (2016).
- R. Belkhou, J. C. Abbé, P. Pham, N. Jasner, J. Sahel, H. Dreyfus, M. Moutaouakkil, R. Massarelli, Uptake and metabolism of boronophenylalanine in human uveal melanoma cells in culture Relevance to boron neutron-capture therapy of cancer-cells. *Amino Acids* **8**, 217–229 (1995).
- H. Maeda, K. Greish, J. Fang, The EPR effect and polymeric drugs: A paradigm shift for cancer chemotherapy in the 21st century. *Polym. Ther. II* **193**, 103–121 (2006).
- T. Tabata, Y. Murakami, Y. Ikada, Tumor accumulation of poly(vinyl alcohol) of different sizes after intravenous injection. *J. Control. Release* **50**, 123–133 (1998).
- I. Rooman, C. Lutz, A. V. Pinho, K. Huggel, T. Reding, T. Lahoutte, F. Verrey, R. Graf, S. M. R. Camargo, Amino acid transporters expression in acinar cells is changed during acute pancreatitis. *Pancreatology* **13**, 475–485 (2013).
- O. Yanagida, Y. Kanai, A. Chairoungdua, D. K. Kim, H. Segawa, T. Nii, S. H. Cha, H. Matsuo, J. Fukushima, Y. Fukasawa, Y. Tani, Y. Taketani, H. Uchino, J. Y. Kim, J. Inatomi, I. Okayasu, K. Miyamoto, E. Takeda, T. Goya, H. Endou, Human L-type amino acid transporter 1 (LAT1): Characterization of function and expression in tumor cell lines. *BBA-Biomembranes* **1514**, 291–302 (2001).
- N. T. Elliott, F. Yuan, A microfluidic system for investigation of extravascular transport and cellular uptake of drugs in tumors. *Biotechnol. Bioeng.* **109**, 1326–1335 (2012).
- H. Cabral, Y. Matsumoto, K. Mizuno, Q. Chen, M. Murakami, M. Kimura, Y. Terada, M. R. Kano, K. Miyazono, M. Uesaka, N. Nishiyama, K. Kataoka, Accumulation of sub-100 nm polymeric micelles in poorly permeable tumours depends on size. *Nat. Nanotechnol.* **6**, 815–823 (2011).
- N. W. Roome, L. Ruttle, L. Williams, W. Smith, The polyvinyl alcohols as blood substitutes. *Can. Med. Assoc. J.* **51**, 293–299 (1944).
- C. C. DeMerlis, D. R. Schoneker, Review of the oral toxicity of polyvinyl alcohol (PVA). *Food Chem. Toxicol.* **41**, 319–326 (2003).
- N. Yamada, Y. Honda, H. Takemoto, T. Nomoto, M. Matsui, K. Tomoda, M. Konno, H. Ishii, M. Mori, N. Nishiyama, Engineering tumour cell-binding synthetic polymers with sensing dense transporters associated with aberrant glutamine metabolism. *Sci. Rep.* **7**, 6077 (2017).
- L. Kou, Y. D. Bhutia, Q. Yao, Z. He, J. Sun, V. Ganapathy, Transporter-guided delivery of nanoparticles to improve drug permeation across cellular barriers and drug exposure to selective cell types. *Front. Pharmacol.* **9**, 27 (2018).
- M. Matsuura, M. Ohshima, Y. Hiruta, T. Nishimura, K. Nagase, H. Kanazawa, LAT1-targeting thermoresponsive fluorescent polymer probes for cancer cell imaging. *Int. J. Mol. Sci.* **19**, E1646 (2018).
- H. Nakamura, N. Ueda, H. S. Ban, M. Ueno, S. Tachikawa, Design and synthesis of fluorescence-labeled *cis*-dodecaborate lipid: Its liposome formation and in vivo imaging targeting of tumors for boron neutron capture therapy. *Org. Biomol. Chem.* **10**, 1374–1380 (2012).
- Y. Matsumoto, J. W. Nichols, K. Toh, T. Nomoto, H. Cabral, Y. Miura, R. J. Christie, N. Yamada, T. Ogura, M. R. Kano, Y. Matsumura, N. Nishiyama, T. Yamasoba, Y. H. Bae, K. Kataoka, Vascular bursts enhance permeability of tumour blood vessels and improve nanoparticle delivery. *Nat. Nanotechnol.* **11**, 533–538 (2016).
- G. Springsteen, B. H. Wang, A detailed examination of boronic acid–diol complexation. *Tetrahedron* **58**, 5291–5300 (2002).
- K. Ono, S. I. Masunaga, Y. Kinashi, M. Takagaki, M. Akaboshi, T. Kobayashi, K. Akuta, Radiobiological evidence suggesting heterogeneous microdistribution of boron compounds in tumors: Its relation to quiescent cell population and tumor cure in neutron capture therapy. *Int. J. Radiat. Oncol., Biol., Phys.* **34**, 1081–1086 (1996).
- K. Ono, S. Masunaga, M. Suzuki, Y. Kinashi, M. Takagaki, M. Akaboshi, The combined effect of boronophenylalanine and borocaptate in boron neutron capture therapy for SCCVII tumors in mice. *Int. J. Radiat. Oncol., Biol., Phys.* **43**, 431–436 (1999).
- K. Ono, H. Tanaka, Y. Tamari, T. Watanabe, M. Suzuki, S. Masunaga, Proposal for determining absolute biological effectiveness of boron neutron capture therapy—The effect

of $^{10}\text{B}(n,\alpha)^7\text{Li}$ dose can be predicted from the nucleocytoplasmic ratio or the cell size. *J. Radiat. Res.* **60**, 29–36 (2019).

35. M. Oliveira, B. S. Barbosa, M. Nele, J. C. Pinto, Reversible addition-fragmentation chain transfer polymerization of vinyl acetate in bulk and suspension systems. *Macromol. React. Eng.* **8**, 493–502 (2014).

Acknowledgments: We thank H. Nakamura, S. Sato, S. Kikuchi, S. Ishii, and F. Nakagawa from Tokyo Institute of Technology for advice on analysis. We appreciate Y. Sakurai, H. Tanaka, and T. Takata in Kyoto University for assistance in neutron irradiation. K. Uehara from Stella Pharma gave insightful advice on the BPA. We thank the Division of Materials Analysis Suzukake-dai, Technical Department, Tokyo Institute of Technology, in particular Y. Sei for the NMR analysis. We received support in proofreading from A. Ghasemizadeh. **Funding:** This work was supported by the Center of Innovation program from the Japan Science and Technology Agency, the Basic Science and Platform Technology Program for Innovative Biological Medicine (JP18am0301008) from the Japan Agency for Medical Research and Development (AMED), the Project for Cancer Research And Therapeutic Evolution (P-CREATE) (JP18cm0106202) from AMED, the Translational Research program: Strategic Promotion for practical application of Innovative medical Technology (TR-SPRINT) (JP19Im0203023), JSPS KAKENHI Grant Numbers 18K18383, 18H04163, and 15H04635, and the Five-star Alliance from the Ministry of Education, Culture, Sports, Science and Technology. **Author contributions:** T.N.

conceived the concept of this study. T.N. and Y.I. designed all the experiments and wrote the manuscript. Y.I. performed all the experiments. T.N. and Y.Y. conducted the in vivo experiments. M.S. performed the neutron capture therapy. K.K. assisted in the in vivo experiments. H.T. advised on the characterization of polymers. M.M. helped in the histological analysis. K.T. advised on the in vivo experiments. T.N. and N.N. supervised the whole project.

Competing interests: Several results presented in this study pertain to our filed patent (2018-028007) in Japan. Y.I., Y.Y., and K.T. are currently employees of JSR Corporation (Tokyo, Japan); this company was not involved in this study. **Data and materials availability:** All data needed to evaluate the conclusions in the paper are present in the paper and/or the Supplementary Materials. Additional data related to this paper may be requested from the authors.

Submitted 19 August 2019

Accepted 25 November 2019

Published 22 January 2020

10.1126/sciadv.aaz1722

Citation: T. Nomoto, Y. Inoue, Y. Yao, M. Suzuki, K. Kanamori, H. Takemoto, M. Matsui, K. Tomoda, N. Nishiyama, Poly(vinyl alcohol) boosting therapeutic potential of *p*-boronophenylalanine in neutron capture therapy by modulating metabolism. *Sci. Adv.* **6**, eaaz1722 (2020).

Poly(vinyl alcohol) boosting therapeutic potential of *p*-boronophenylalanine in neutron capture therapy by modulating metabolism

Takahiro Nomoto, Yukiya Inoue, Ying Yao, Minoru Suzuki, Kaito Kanamori, Hiroyasu Takemoto, Makoto Matsui, Keishiro Tomoda and Nobuhiro Nishiyama

Sci Adv 6 (4), eaaz1722.

DOI: 10.1126/sciadv.aaz1722

ARTICLE TOOLS

<http://advances.sciencemag.org/content/6/4/eaaz1722>

SUPPLEMENTARY MATERIALS

<http://advances.sciencemag.org/content/suppl/2020/01/17/6.4.eaaz1722.DC1>

REFERENCES

This article cites 35 articles, 0 of which you can access for free
<http://advances.sciencemag.org/content/6/4/eaaz1722#BIBL>

PERMISSIONS

<http://www.sciencemag.org/help/reprints-and-permissions>

Use of this article is subject to the [Terms of Service](#)

Science Advances (ISSN 2375-2548) is published by the American Association for the Advancement of Science, 1200 New York Avenue NW, Washington, DC 20005. The title *Science Advances* is a registered trademark of AAAS.

Copyright © 2020 The Authors, some rights reserved; exclusive licensee American Association for the Advancement of Science. No claim to original U.S. Government Works. Distributed under a Creative Commons Attribution NonCommercial License 4.0 (CC BY-NC).